# Local Interfacial Migration of Clay Particles within an Oil Droplet in an Aqueous Environment

*Kyongok Kang*[*1], *J. S. Hong*[2], *and J. K. G. Dhont*[1]

[1] Forschungszentrum Juelich, ICS-3 (Soft Condensed Matter), Juelich, 52425, Germany

[2] Departments of Chemical Engineering, Soongsil University, Seoul, South Korea

ABSTRACT

We discuss the interfacial migration due to Marangoni forces of clay particles within an oil droplet that is immersed in water, which is relevant for the formation kinetics of Pickering emulsions. Hydrophilic (MMT) and hydrophobic (OMT) clays are studied, where the hydrophilic clay particles adsorb in the oil-water interface, contrary to the hydrophobic clays. The feasibility of an "image time-correlation technique" is discussed, in order to probe the local interfacial migration velocities of clay particles in the oil droplet. Here, correlation functions are constructed from time-resolved images, in order to quantify the local migration of clay particles. Correlation functions are measured at different waiting times, that is, the time after formation of the droplet. The initial decay rate and the baseline of these correlation functions depend on the waiting time in a qualitatively different way for the two clays, which is attributed to the different interfacial migration behavior for the hydrophilic, adsorbing clays, and the non-adsorbing, hydrophobic clays as a result of the Marangoni effect.

KEYWORDS

Interfacial layer, Migration velocity, Image-time correlation, Marangoni effect, Pickering emulsions

## INTRODUCTION

Emulsions consisting of thermodynamically immiscible components can be stabilized by colloidal particles that are located within the interfacial layer. The particle-laden interfacial layer of these so-called Pickering emulsions prevents coalescence of droplets [1-7]. Typically, emulsions are fabricated by turbulent mixing for a short time, which are subsequently stable for long times in the quiescent state. The kinetic pathway to prepare Pickering emulsions is crucial for their long-term stability. Under flow conditions like for turbulent mixing, the temporal evolution of micro-structural order of the emulsion is largely determined by hydrodynamic flow, while particle mass transport due to surface-tension gradients and diffusion close to and within the interface can also play a role. For large Peclet numbers, which measures the relatively importance of convection as compared to diffusion, motion of the particles away from the interface within the bulk is dominated by flow. Particles within the bulk then follow the flow lines of the surrounding fluid [8]. After vigorous emulsification, micro-structural order will change preliminary by diffusive mass transport. In addition to diffusion, mass transport due to sedimentation may also play a role. An understanding of the dynamics of Pickering particles in emulsions is therefore necessary to be able to predict the nature of Pickering-emulsion formation and to design emulsions for diverse industrial applications. In this paper, we investigate the dynamics of clay particles within an oil droplet, embedded in water [9]. Such mineral inorganic particles are known to inherently stabilize emulsions resulting from their ionic surface

characteristics [10, 11]. The aim of this paper is to establish the feasibility of an image time-correlation technique [12, 13] in order to quantify local migration of clay particles within an oil droplet, after the formation of the oil droplet. Here, image time-correlation functions are constructed from time-resolved microscopy images, where the initial decay rates of correlation functions will be shown to measure the velocities of particles, while their baseline measures the local particle concentration. Two types of clays are considered: one is a sodium montmorillonite (MMT) clay, the other clay is organically modified MMT that is be referred to as OMT. MMT-clay adsorbs at the oil-water interface, while the OMT is a hydrophobic and that does therefore not adsorb. In the clay-particle systems under investigation here, aggregates are formed in bulk and the motion of such heavy particles is significantly affected by gravity [14]. The relative importance of sedimentation and diffusion is quantified through a Peclet number that is equal to the ratio of time required to diffuse over a distance equal to the size of the aggregates, and the time required to sediment over that distance. Thus, for heavy large particles with a large Peclet number, i.e., Pe>1, the motion is not purely diffusive but is significantly affected by sedimentation. The clay-aggregates tend to move along the direction of gravity, affected by the curved oil-water interface when they are in the vicinity of the interface, and accumulate at the rear end of the oil droplet. Depending on whether the clays are adsorbed in the interface or not, both the migration of particles and their concentration will gradually change in time. Mass fluxes near the oil-water interface are expected to be different for MMT-clay and OMT-clay particles, as the former adsorbs at the interface and the latter does not. The adsorption characteristics in turn depend on the interfacial adsorption energy of the clays surrounded by oil or water. In addition, in the initial stages of Pickering formation, there are concentration gradients along the interface, depending on the type of clays. A simple schematic drawing is shown in Figure 1 to

illustrate the various stages during Pickering formation under gravity. Just after injection of the suspension of clay particles dispersed in the oil droplet into the water, the spatial variation of the concentration distribution will change in time due to both diffusion and sedimentation. When clays adsorb, there will in addition be a Marangoni flux along the interface towards the upper region of the oil droplet [15]. This can be observed by the migration of particles close to and within the curved oil-water interface. Particles in the vicinity of the interface will move upwards due to the flow induced by the motion of the adsorbed clay particles within oil-droplet/water interface.

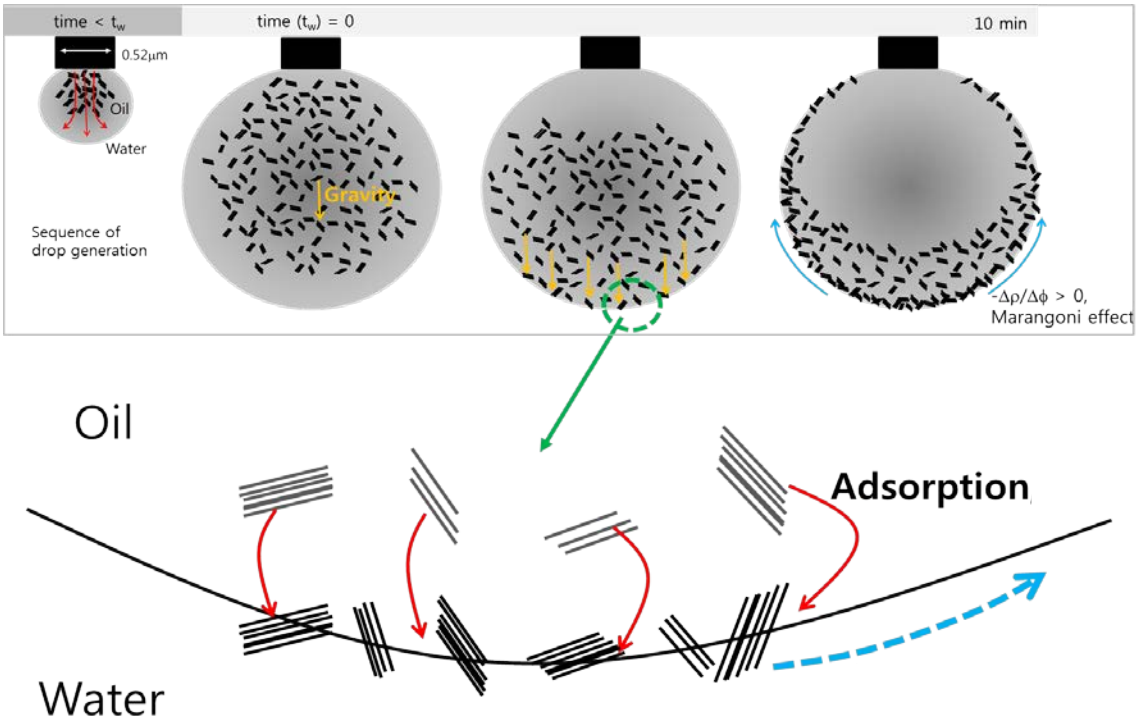


Figure 1: A sketch of clay migration to the curved oil-water interface and interfacial layer formation (Pickering). MMT clay particles adsorb at the interface when their wettability of oil relative to water is such that adsorption leads to a decrease of the interfacial free energy.

After a certain time (~25-30 min), sedimentation leads to an accumulation of clays at the rear end of the droplet. For strongly adsorbing particles (the MMT-clays) the interface will be homogeneously covered in the final steady state, while for non-adsorbing particles (the OMT-clays) an inhomogeneous particle distribution will exist.

## MATERIALS

Canola oil (CJ Cheil-Jedang Co., Korea) is used as the dispersing oil phase, which mostly consists of unsaturated fatty acids (91.3 %). The oil has a density of 0.85 g/ $cm^3$ and a viscosity of 0.06 Pas. As the continuous phase, purified (Barnstead RO pure LP system, Thermo Scientific, USA) and deionized (Nanopure II systems, Thermo Scientific, USA) water was used. Two types of nano-clay particles (Southern Clay Products Inc, USA) with different surface characteristics are used: sodium montmorillonite (MMT) which is hydrophilic, and organically modified MMT which is hydrophobic. The hydrophilic clay MMT has sodium ions on the surface, as a natural silicate, and its density is 2.6 g/$cm^3$. The organically modified MMT (Closite 20A) is a dimethyl hydrogenated-tallow ammonium modified MMT, to which we will refer to as the OMT clay. The hydrophobic clay OMT has a density is 1.7 g/$cm^3$. These particles were prepared by exchanging the ions in sodium MMT by alkyl ammonium cations. Clay particles (3000 ppm) are dispersed in the oil phase using a magnet stirrer. To avoid large changes of the degree of aggregation during observation, clays were stirred in the oil for 5 hours at room temperature and observed within 1 day. The experimental scheme of the oil droplet formation in the water reservoir is shown in Figure 2a, where the inner and outer diameter of the syringe needle is indicated in the top right (the inner diameter is 0.26 mm, the outer diameter 0.52 mm).

Figure 2b is a movie that shows the formation of the oil droplet on injection in the water bath. The oil phase is pushed into the water phase with a slow volumetric flow rate of 1 $\mu l$ /min. The typical final oil droplet diameter is about 1.5 mm, with a volume of 1.2 $\mu l$ . The gravitation direction is from top to bottom, along the alignment of the syringe. The oil drop is monitored for two hours after drop formation through a microscope (Olympus SZ61, 25x lens, Japan). Both types of clay particles are present in the form of aggregates with a size of a few microns. Due to their hydrophobic nature, the OMT clays are less aggregated and more homogeneously distributed. The size of the particle aggregates of MMT and OMT clays are of the order of 30 $\mu m$ and 20 $\mu m$, respectively.

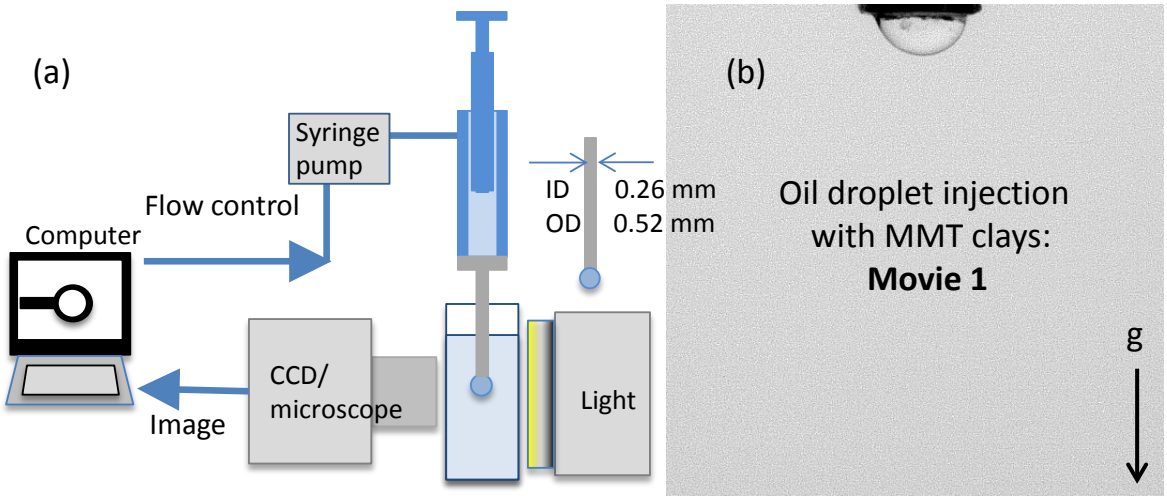


Figure 2: (a) Schematic of the equipment for a drop formation and observation, where the drop (1.2ml) maintains attached at the end of a syringe needle (0.52mm in outer diameter). The dimension of container is 10 x10 x 45 mm (width, depth, height). (b) The formation of an oil droplet is shown in **Movie 1**.

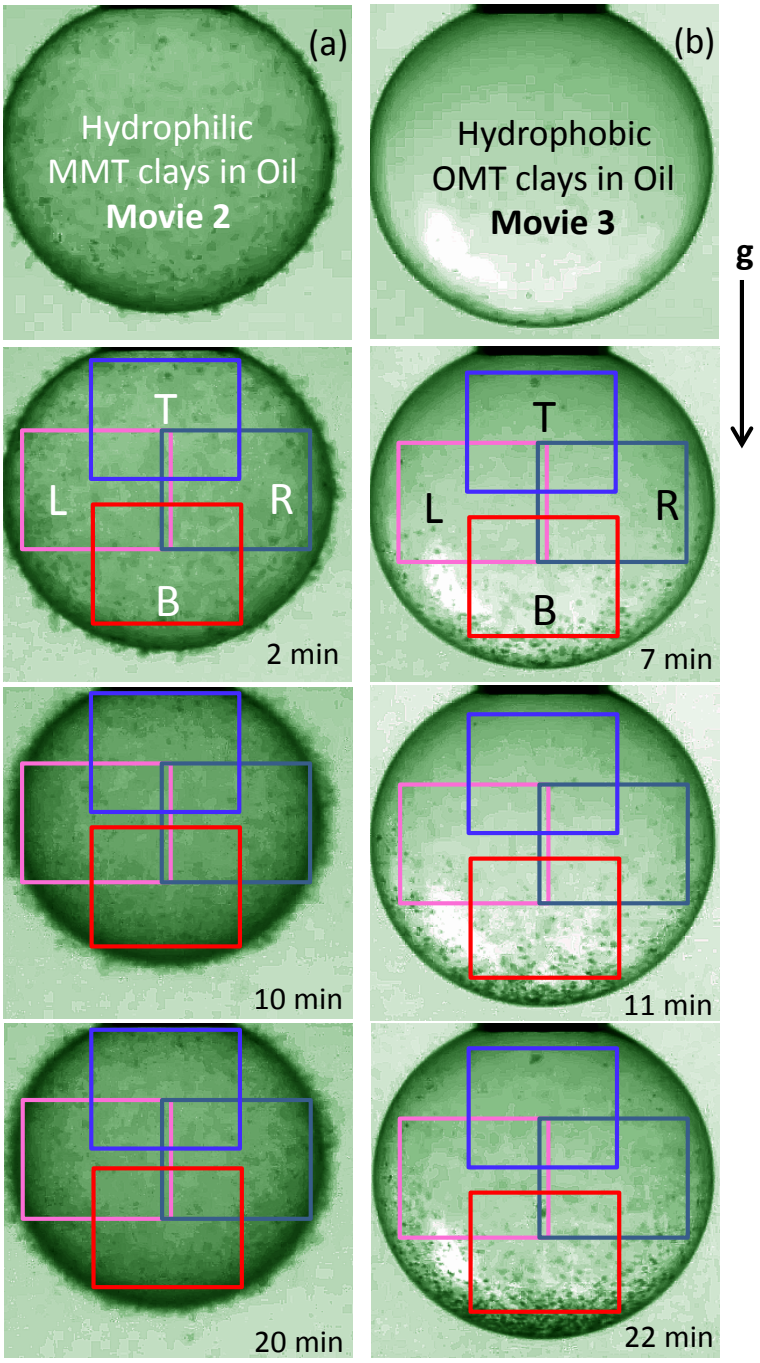


Figure 3: Spatio-temporal images for (a) hydrophilic MMT-clays, and (b) hydrophobic OMT-clays in an oil drop, for several waiting times $t_w$ , as indicated in the figures. The top panels are **Movie 2** and **Movie 3,** respectively. The different regions of interest (ROIs) are indicated as a square (120x120 pixels).

METHODS: IMAGE TIME-CORRELATION FUNCTIONS

We apply an image time-correlation technique for both types of clays to quantify the properties of migration of clays within the oil droplet that is embedded in water. Different regions of interest (ROI) are chosen for the image-time correlation data analysis. First the collection of time-resolved video data is required to extract time-lapsed images with an optimized time binning and spatial resolution for the analysis of the time-dependent positions of clay particles. A useful criterion for the time resolution of subsequent images is a time binning with a time-interval that is 10 times shorter than the actual dynamical events. As will be discussed below, time-correlation functions will be constructed from these images, the initial slope of which measure the average magnitude of particle velocities within the field-of-view. PIV would be an alternative method to obtain local velocities, both in magnitude and direction. The advantage of our method is that it is can be used for very dilute systems, it is very easy to implement, and does not require the optics that is necessary to perform PIV measurements. Also, the image-time correlation technique measures average velocities over regions with a size that can be chosen such that it gives a reasonable spatial resolution, and averages-out variations in velocities that are not of interest, like variations of velocities due to interactions between particles. Spatio-temporal images of both hydrophilic MMT clays and hydrophobic OMT clays in an oil droplet that is immersed in the water reservoir are shown in Figure 3, where the top panels correspond to **Movie 2** and **Movie 3,** respectively (these movies can be found in the supplementary material). The different regions of interest (ROI) that we probe are indicated as squares (of 120x120 pixels). Time-lapsed enhanced contrast images of data movies are shown in Figure 3, for both clays, taken a few minutes after the droplet is created. The left panel shows the hydrophilic MMT clay particles, and the right panel shows the hydrophobic OMT particles, while the

sedimentation direction is downwards, indicated by the arrow. As can be seen in the Movie 2 of Figure 3 (a), the MMT clays adsorb in the interface are tend to move upwards with a slight shrinkage of the oil droplet, contrary to the OMT clays. The interest here is in the trajectories of different types of clay particles within the various ROIs, indicated by the squares in Figure 3, where B, T, R, and L, refer to Bottom, Top, Right, and the Left ROI respectively. The aim is to extract differences in the image time-correlation functions within these four ROIs between the clay particles that adsorb. To construct image-time correlation functions, time-resolved images of the transmitted intensity are collected with a CCD camera, and the images are enhanced such that the clay particles appear white and the background black. From these images, image time-correlation functions are constructed, which are defined as,

$$C_V(t) = \frac{\left\langle \left[ I(t) - \langle I(t) \rangle \right] \left[ I(0) - \langle I(0) \rangle \right] \right\rangle}{\left\langle \left[ I(0) - \langle I(0) \rangle \right]^2 \right\rangle}, \qquad (1)$$

where $I(t)$ is the intensity of a pixel at time $t$, while the brackets $\langle \cdots \rangle$ indicate averaging over all pixels.

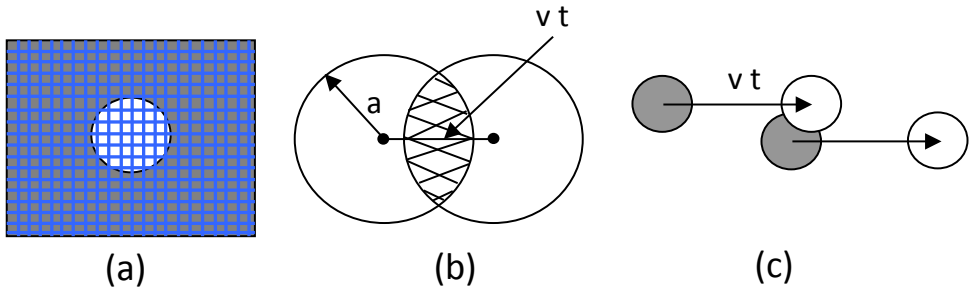


Figure 4: (a) An image of a clay particle on the CCD-camera chip. Each little square is a pixel. (b) The clay particle at two different times. The image time-correlation function at time t measures the shaded overlap area of the two corresponding images at that time (for mathematical details, see the Appendix). (c) At later times, the time dependence of the image time-correlation function is determined by the overlap of areas of different particles.

Consider a single particle that moves with a velocity **v** within the plane of detection. Let *S* be the projected area of the particle within the plane-of-view. This area covers several pixels of the CCD camera, as sketched in Figure 4a, where the particle is assumed to be spherically symmetric. Since in the images the particles are made bright, the excess intensity $I_i$ of a pixel number *i* with position $\vec{r}_i$ of the centers of a sphere within the two-dimensional field-of-view is proportional to the characteristic function $\chi(\vec{r}_i)$ of the white surface area *S*, where $\chi(\vec{r})$ =1 for $\vec{r} \in S$ and $\chi(\vec{r}) = 0$ otherwise. The location of the surface area *S* is time dependent as the particle moves with velocity **v**. The image time-correlation function is thus equal to (with $t_W$ as the waiting time, at which the measurement is started), $C_V(t) \sim I(t_w)I(t_w + t) \sim \int d^3 r \chi(r)\chi(r + vt)$, where the integral ranges over all pixel positions within the field-of-view. The integral is equal to the surface area of overlap of two disks, assuming spherical particles, as sketched in Figure 4b. The distance between the two disks is equal to $\Delta r = v\,t$. As shown in the Appendix, this leads to,

$$C_V(t) \sim \mathrm{a}^2 \cos^{-1}\left(\frac{vt}{2a}\right) - \frac{1}{2}(vt)^2 \tan\left(\cos^{-1}\left(\frac{vt}{2a}\right)\right), \qquad (2)$$

where *a* is the radius of the spherical particle. Expanding with respect to $v\,t\,/\,a$, and normalizing to unity at time $t = 0$ leads to,

$$C_V(t) = \frac{I(t_W)\,I(t + t_W)}{I^2(t_W)} = 1 - \frac{vt}{2a} + \mathrm{O}(t^2). \qquad (3)$$

$\mathrm{O}(t^2)$ represents terms of order $t^2$. The initial slope of the correlation function is thus a measure for the magnitude of the velocity of the particles. As the image time-correlation technique measures only the magnitude of velocities, the direction of velocities is determined separately by

the given movie data from which correlation function are constructed. At later times, overlap between different particles occurs (as depicted in Fig.4). Such events determine the long-time behavior of the correlation functions.

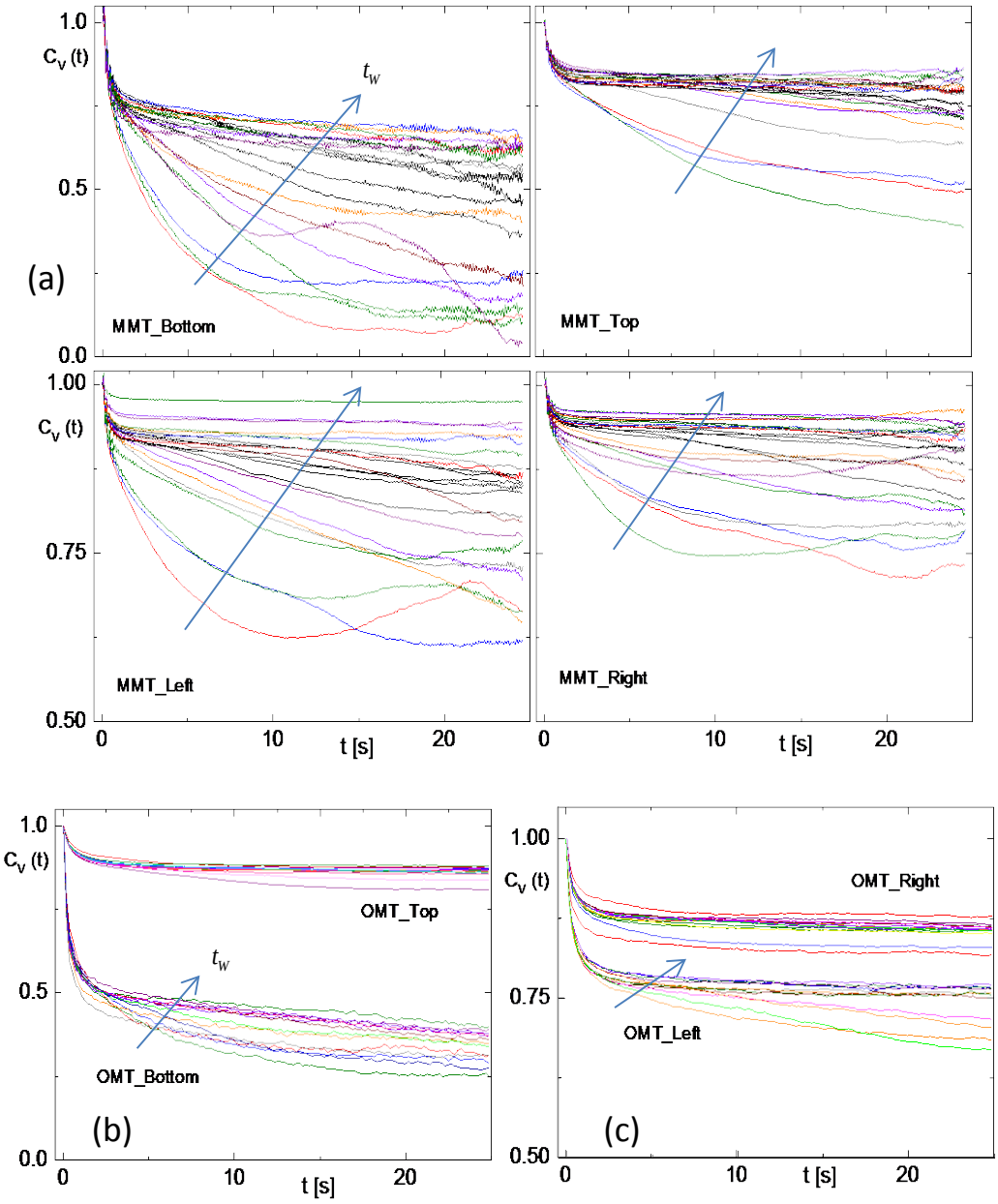


Figure 5: Image time-correlation functions of (a) the hydrophilic MMT clay, (b) and (c) for hydrophobic OMT clay, for the different ROIs (Regions Of Interest) and for various waiting times, increasing in steps of 25s. The arrows indicate increasing waiting time.

The assumption in the above analysis is that no overlap occurs of images of different particles for short times. Nevertheless, the initial slope of time-correlation functions is a measure for the migration of particles within the probed ROI. The difference between the above idealized theory and our measured correlation functions is the due to presence of constant background intensity. Due to the background intensity, correlation functions typically do not decay to zero for longer times. There is an unavoidable static background intensity that does not originate from the clay particles, and there may be a part that comes into play that is due to immobile clay particles. The relative contribution of the static background intensity becomes more important as less mobile clay particles are present. An increasing value of the baseline is therefore interpreted as a decrease of the concentration of mobile clay particles within the ROI. Since the distance between particles is much larger than the size of the particles, there is a well-separated time regime between the initial slope where eqns. (2, 3) are valid and later times where areas of different particle begin to overlap. Thus image time-correlation functions typically do not decay to zero for longer times due to unavoidable static background intensity. The relative contribution of the static background intensity becomes more important as less clay particles are in motion, leading to an increase of the base line. The value of the base line, especially its temporal change, is thus (a crude) measure for the concentration of mobile clay particles. Four different ROIs are indicated by the squares in Figure 3, which comprise 120 x 120 pixels: a region at the top, close to the droplet entrance, a region near the bottom part of the droplet, and regions in the middle on the left and the right. The image time-correlation functions of both clays are shown in Figure 5, for various waiting times, where the initial slope of these correlation functions, as discussed above, measures the average motion of migration. Here, images are collected for about 10 min,

comprising 300 image time frames, and the image time-correlation functions are calculated with a time binning of 25 s for the MMT-clays (in Figure 5(a)), and 55s for the OMT-clays (in Figure 5(b) and (c)). The length conversion of regions of view is 4.64 $\mu m$/pixel, and 4.56 $\mu m$/pixels, for MMT and OMT clays, respectively. The difference in this length conversion is due to a slightly different size of the oil droplet in both cases. The arrows indicate the increase of waiting time $t_w$ in Figure 5.

RESULTS

From the top four panels in Figure 5(a), in image time-correlation functions for the MMT clays, and the two lower panels in Figure 5(b) and 5(c) for the OMT clays, it is clear that the waiting-time dependence of the correlation functions in the various regions of interest (ROIs) for the MMT and OMT clays are quite different. The initial decay of the correlation functions can be fitted with a single stretched exponential as $C_V(t) = A\exp\left\{-(\Gamma t)^{\beta}\right\} + B$ , where the amplitude *A*, the base line *B*, the decay rate $\Gamma$, and the stretching exponent $\beta$ are fitting parameters (for normalized correlation functions, *B=1-A*).

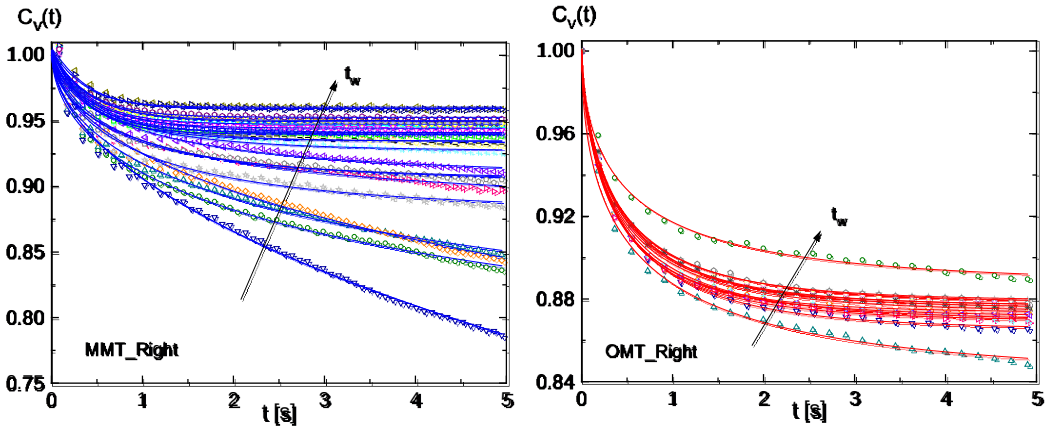


Figure 6: An example of the fitting of correlation functions for the right-ROI: left for MMT clays, and right for the OMT clays. The solid lines are fits to the stretched exponential discussed in the main text.

Examples of the fitting results of the initial decay of correlation functions are shown for the right-ROI for both clays in Figure 6. A can be seen, the stretched exponential function fits the data quite accurately. As mentioned above, the initial decay rate $\Gamma$ is a measure for the average migration velocity of the particles within the probed ROI, while the amplitude A=1-B decreases as the concentration of mobile particles decreases (the baseline *B* increases). A stretched exponential is used as a functional form to describe the decay of the correlation function over an extended time range, and thereby extract accurate values for the initial slope. The origin of the stretched exponent is that it represents the higher order terms in time in eq.3, and the overlap of different particles at later times. In light scattering experiments, $\beta$ is usually taken as a measure for the polydispersity of the particles, as the higher order terms in time that give rise to a value of $\beta$ below unity originate from polydispersity. In our case, in addition to polydispersity, such higher order terms in time are also present for monodisperse particles (see eq.3). We will therefore not use $\beta$ in the sequel as a measure for polydispersity, but regard it simply as a parameter that is included in fits to extract accurate values for the initial slope of correlation functions.

The fitting results of the amplitude and stretching exponent are given in Figure 7(a), and (b), respectively, where the left panels are for the MMT clays, and the right panels for the OMT clays. As can be seen, there is marked difference between the correlation functions as a function waiting time for the two clays, both for the initial waiting times ($t_w < 200\,s$) and later times ( $t_w > 200\,s$). From Figure 7(a), a significant decrease of the amplitude (*A=1-B*, where *B* is the base line) is found for the MMT clays (left panel) within the first 200 s after formation of the droplet, whereas an essentially constant amplitude is found for the OMT clays (right panel). As

discussed above, this implies a diminishing particle concentration for the MMT clays. This is attributed to adsorption, by which particles disappear from the ROIs. The amplitudes for the OMT clays remain constant, as the increase of the concentration due to sedimentation is relatively small during the measuring time. Note that the observed temporal increase of the stretching exponent $\beta$ for the MMT clays cannot be explained in terms of changes in polydispersity, as mentioned above.

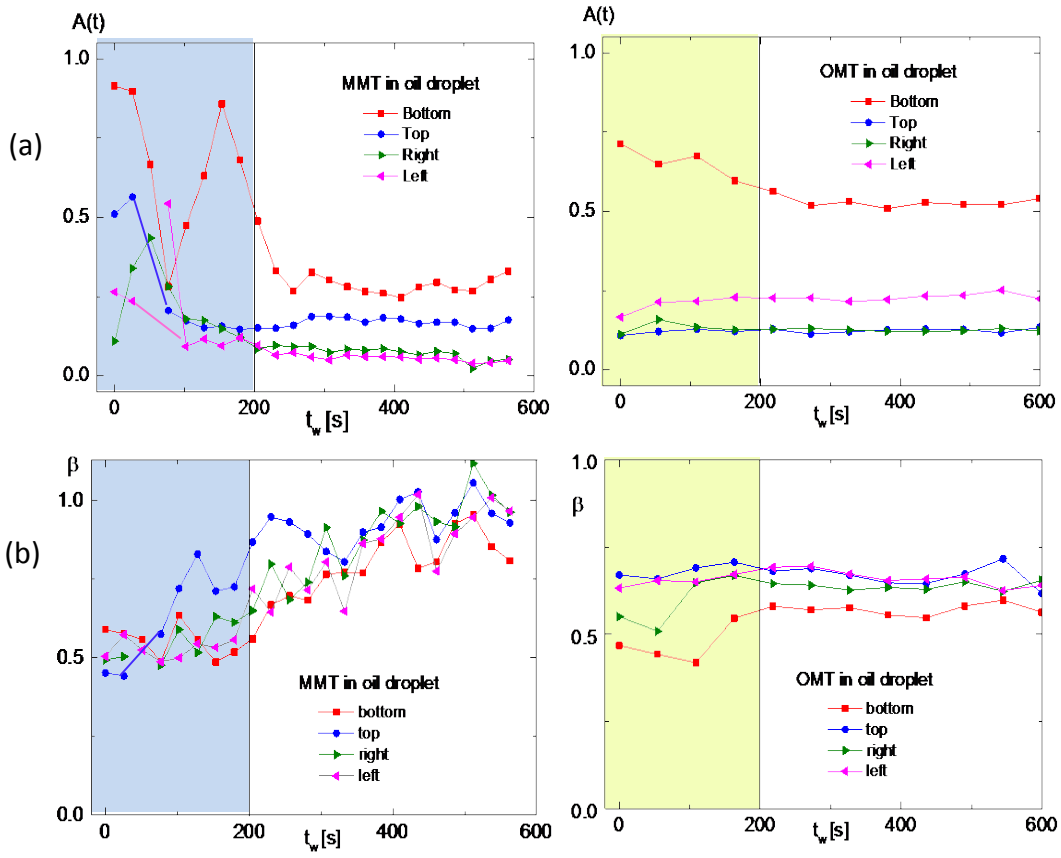


Figure 7: The comparison of migration for MMT-clays (left) and OMT-clays (right) at different ROIs as a function of waiting time $t_w$: (a) the amplitude, (b) the stretching exponent.

Furthermore, the interfacial migration of the MMT clays, as can be seen the left of Fig.8, increases with increasing waiting time up to 200 s, for all four ROIs, which is again in contrast to what is seen for the OMT clays (in the right of Figure 8), in particular the bottom and top ROIs. The increasing average migrations for the MMT clays are attributed to the Marangoni effect, where motion of particles within the interface drags particles in the vicinity of the interface along through the induced flow. The Marangoni-induced migrations are apparently much stronger than typical sedimentation velocities, which determine the initial values to the decay rates before adsorption occurred. The sedimentation velocities of the MMT and OMT clays are estimated from the earlier mentioned mass densities and their approximate sizes of 15 $\mu m$ and 10 $\mu m$ radius, as 15 $\mu m / s$ and 3.3 $\mu m / s$, respectively. The estimated sedimentation velocities of the MMT and OMT clays are indeed quite small compared to the Marangoni-induced back flow for the MMT clays, and also lower than that of typical values for the OMT clays. A quasi-stationary state is reached for waiting times larger than about $t_W > 200 s$. Most intriguing founding from our image time-correlation is that the decay rates for all four ROIs are very similar for the MMT

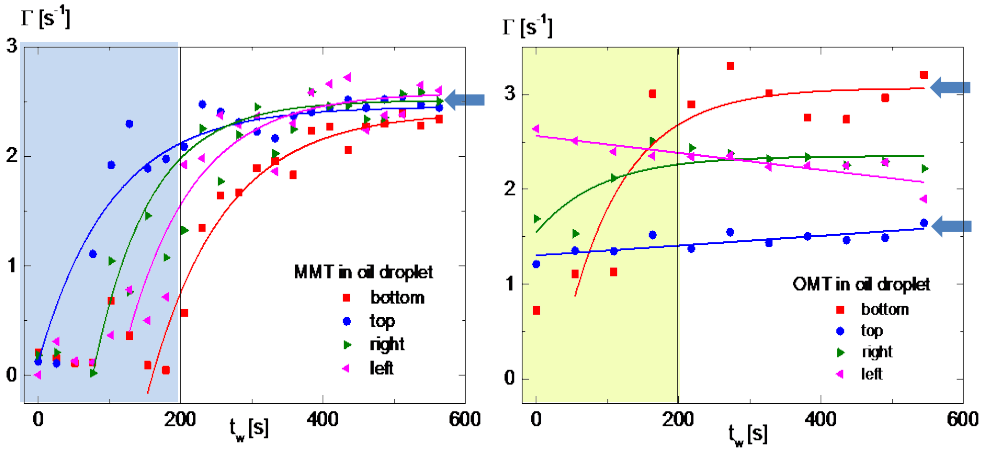


Figure 8: The comparison of initial decay rates for MMT-clays (left) and OMT-clays (right) at different interfacial migration ROIs as a function of waiting time $t_w$.

clays (indicated with an blue arrow in the left Figure 8), which strongly supports that the local migrations are indeed dominated by Marangoni flow.

The OMT clays, on the contrary, exhibit a qualitatively different behavior. The initial decay rates are essentially independent of the waiting time (see the right panel in Figure 8), except for the bottom ROI. The top ROI exhibits a relatively low, constant decay rate at early waiting times. At long times, two distinct values of decay rates are observed, a relatively large value for the bottom ROI, and a lower value for the other ROIs (as indicated by the two arrows in the right of Figure 8). The large decay rate at the bottom is probably due to accumulation of clay particles due to sedimentation, where interactions between them enhance their relative motion. To within the admittedly large errors, the particles in the right and left ROIs migrate with the same velocity, as they should by symmetry.

**Conclusion and Discussion**

We demonstrated the use of image time-correlation to characterize the local interfacial migration of clay particles within an oil-droplet in an aqueous environment. Local migrations within a Region Of Interest (ROI) can be determined from the initial slope and the baseline of image-time correlation functions. We have successfully shown that image time-correlation functions taken at various waiting times after formation of the oil droplet and at different ROIs reveal the influence of the Marangoni effect on the migration velocities of the hydrophilic MMT clay particles, which adsorb at the oil-water interface, contrary to the non-adsorbing hydrophobic OMT clays. Local migrations within a Region Of Interest (ROI) can be determined from the initial slope of image time-correlation functions, while their constant value at large times can be used as an indicator for the concentration of mobile clay particles: a higher value of the base line of correlation functions is due to a lower concentration of mobile clay particles. Flow that is

induced by rising particles within the interface due to Marangoni forces cause particles at the sides of the droplet to attain a relatively large velocity as compared to their sedimentation velocity.

It would be worthwhile to formulate a convection-diffusion equation and boundary conditions, including an appropriate model for the adsorption kinetics and the Marangoni effect, in order to quantify the entire Pickering process. Such an endeavour has not been undertaken yet. Finally, the use of image-time correlation to probe particle migration is not limited to the clay system studied here, but may be more generally applicable to probe flow patterns in inhomogeneously flowing systems containing mesoscopic objects.

ACKNOWLEDGMENT

JS Hong acknowledges the support by Mid-career Researcher Program through NRF grant (No. 20110016890) funded by the Korea government (MEST).

APPENDIX

To arrive at eq.2 for the correlation function, we need to evaluate the integral $C_V(t) \sim I(t_w)I(t_w+t) \sim \int d^3r\chi(r)\chi(r+vt)$. The integrand is the overlap area of two disks that are separated by a distance *vt* (as shown in Figure 9). This area is equal to,

$$C_V(t) \sim 2\int_{-\theta_m}^{\theta_m} d\theta \int_{\frac{vt}{\cos\theta_m}}^{a} dl\, l = 2a^2\left[\theta_m - \left(\frac{vt}{2a}\tan\theta_m\right)\right]$$

where $\theta_m$ is the maximum of the angle $\Theta$ in Figure 9,

$$\cos\theta_m = \frac{vt}{2a}$$

Combination of the two above equations leads to eq.2. Using that,

$$\cos^{-1}\varepsilon = \frac{\pi}{2} - \varepsilon + \cdots \quad ,$$

$$\varepsilon^2 \tan\left(\frac{\pi}{2} - \varepsilon\right) = \varepsilon + \cdots \quad .$$

where $\varepsilon = \frac{vt}{2a}$ we arrive at eq.3 for the normalized correlation function (which is unity at time zero).

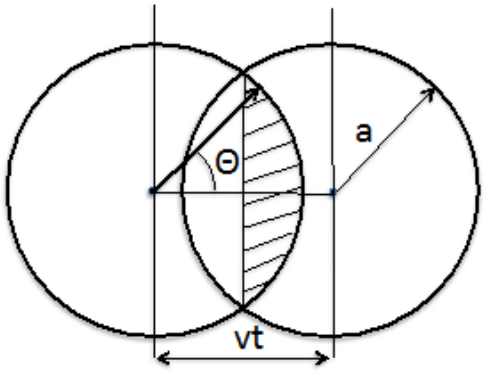


Figure 9: The overlap area (which is twice the shaded area) of two disks separated with their centers-of-mass by *vt*, is equal to the image time-correlation function.

REFERENCES

[1] Ramsden, W, Separation of Solids in the Surface-Layers of Solutions and 'Suspensions' (Observations on Surface-Membranes, Bubbles, Emulsions, and Mechanical Coagulation), Proc. R. Soc. Lond. **1903**, 72, 156-164

[2] Pickering, S.U. Emulsions, J. Chem. Soc. **1907**, 91, 2001

[3] Binks, B.P.; Horozov, T.S. Colloidal particles at liquid interfaces, Cambridge University Press, UK, **2006**

[4] Kralchevsky, P.A.; Ivanov, I.B.; Ananthapadmanabhan, K.P.; Lips, A. On the thermodynamics of particle-stabilized emulsions: curvature effects and catastrophic phase inversion. Langmuir **2005**, 21, 50-63

[5] Hunter, T.N.; Pugh, R.J.; Franks, G.V.; Jameson, G.J. The role of particles in stabilizing foams and emulsions. Adv. Colloid Int. Sci. **2008**, 137, 57-81

[6] Binks, B.P.; Rocher, A.; Kirkland, M. Oil foams stabilized solely by particles. Soft Matter **2011**, 7, 1800

[7] Levine, S.; Sanford, E. Stabilization of emulsion droplets by fine powders, Canadian J. Chem. Eng. **1985**, 63, 258-268

[8] Larson, R.G. The structure and rheology of complex fluids. Oxford University Press, New York **1999**.

[9] Kim, J.K.; Ruhes, P.A.; Fischer, P. Interfacial localization of nanoclay particles in oil-in-water emulsions and its reflection in interfacial moduli. Rheol. Acta **2013**, 53, 327-335

[10] Tsugita, A.; Takemoto, S.; Mori, K.; Yoneya, T.; Otani, Y. Studies on O/W emulsions stabilized with insoluble montmorillonite-organic complexes. J. Colloid Int. Sci. **1983**, 95(2):551-560

[11] Behin, J.; Norouzi S. Influence of water ions and aluminum silicate particles on emulsion resolution of crude oil. Petroleum & Coal **2011**, 53(2):115-122

[12] Kang, K; Dhont, J.K.G. Electric-field induced transitions in suspensions of charged colloidal rods. Soft Matter **2010**, 6, 273-286

[13] Kang, K. Image time-correlation, dynamic light scattering, and birefringence for the study of the response of anisometric colloids to external fields. Rev. Sci. Instrum, **2011**, 82, 053903

[14] Hong, J.S.; Kim, J.G. Variation of interfacial tension by nanoclay particles in oil-in-water emulsions, Composite Interfaces, 2014,1-11 (DOI:10.1080/15685543.2014.928580)

[15] Marangoni, C. G. M., Ueber die Ausbreitung der Tropfen einer Flussigkeit auf der Oberflache einer anderen, Ann. Phys. Chem. (Poggendorff), **1871**, 143(7), 337

ASSOCIATED CONTENT

**Supporting Information**. A brief statement in non-sentence format listing the contents of material supplied as Supporting Information should be included, ending with “This material is available free of charge via the Internet at http://pubs.acs.org.”

A brief statement of Movie descriptions:

**Movie 1**: The formation of an oil droplet that is immersed in a quiescent water reservoir. The gravitation direction is on the right side.

**Movie 2**: Enhanced speed up movie data of the hydrophilic MMT clays in the oil droplet that is immersed in a water reservoir. The total time is about 20 min, and a field-of-view of 300 x300 pixels. The image-time correlation is performed for a field-of-view of 120x120 pixels, located at different positional ROIs. The corresponding length calibration is 4.64 um/pixel. The gravitation direction is on the right side.

**Movie 3**: Enhanced speed up movie data of the hydrophobic OMT clays in the oil droplet immersed in a water reservoir. The total time is about 22 min, and a field-of-view as 300 x300 pixels. The image-time correlation is performed for a field-of-view of 120x120 pixels, located at different positions. The corresponding length calibration is 4.56 um/pixel. The gravitation direction is on the right side.

AUTHOR INFORMATION

**Corresponding Author**

* Kyongok Kang is the corresponding author.

**Author Contributions**

The manuscript was written through contributions of all authors. All authors have given approval to the final version of the manuscript. ‡These authors contributed equally.

**Funding Sources**

JS Hong acknowledges the support by Mid-career Researcher Program through NRF grant (No. 20110016890) funded by the Korea government (MEST).

**TOC:**

A sketch of clay migration to the curved oil-water interface and interfacial layer formation (Pickering). MMT clay particles adsorb at the interface when their wettability of oil relative to water is such that adsorption leads to a decrease of the interfacial free energy.